

DAYTIME MUD DETECTION FOR UNMANNED GROUND VEHICLE AUTONOMOUS NAVIGATION

A. L. Rankin* and L. H. Matthies
Jet Propulsion Laboratory, California Institute of Technology
4800 Oak Grove Drive, Pasadena, CA, USA 91109

ABSTRACT

Detecting mud hazards is a significant challenge to UGV autonomous off-road navigation. A military UGV stuck in a mud body during a mission may need to be sacrificed or rescued, both unattractive options. JPL is currently developing a daytime mud detection capability under the RCTA program using UGV mounted sensors. To perform robust mud detection under all conditions, we expect multiple sensors will be necessary. A passive mud detection solution is desirable to meet the FCS-ANS requirements. To characterize the advantages and disadvantages of candidate passive sensors, data collections have been performed on wet and dry soil using visible, multi-spectral (including near-infrared), short-wave infrared, mid-wave infrared, long-wave infrared, polarization, and stereo sensors. In this paper, we examine the cues for mud detection each of these sensors provide, along with their deficiencies, and we illustrate localizing detected mud in a world model that can be used by a UGV to plan safe paths.

1. INTRODUCTION

There are many types of terrain (such as, pavement, gravel, firm dirt, mud, snow, ice, water, and vegetation of varying height and thickness) that an unmanned ground vehicle (UGV) can encounter during autonomous navigation over cross country terrain. The ability to detect and avoid hazardous terrain poses a current challenge to the acceptance and proliferation of tactical UGVs (Mills, 2007). Since water and mud are prevalent in many regions during the entire year, robust detection of those hazards is a critical perception requirement for UGV autonomous navigation.

Water and mud bodies need to be detected at a sufficient distance (which is a function of the UGV's current speed) that allows the UGV to evade it. A UGV that becomes stuck in water or mud during an in-theater autonomous mission may require rescue, potentially drawing critical resources away from the primary mission and soldiers into harms way. Under the Army Research Laboratory (ARL) Robotics Collaborative Technology Alliances (RCTA) program, the Jet Propulsion Laboratory (JPL) is developing a water and mud detection capability for UGVs. At the last Army Science Conference, we reported our progress on detecting and localizing water

bodies in a world model used to plan safe paths (Rankin and Matthies, 2006). This year, we report our progress on evaluating sensors applicable to mud detection from an UGV.

Figure 1 illustrates the class of UGV this work is being performed for and a severe mud hazard from a test site near General Dynamics Robotic Systems, Westminster, MD. Although mud detection for UGV autonomous navigation is a relatively new research area, techniques to estimate soil moisture content have been studied for decades for agricultural applications (Hamrita et al., 2000). Soil moisture content has been estimated using devices requiring contact with the ground and via remote sensing (Whalley and Stafford, 1992; Suddeth et al., 1997).



Figure 1. An experimental unmanned vehicle (XUV) navigating through a muddy grass field near General Dynamics Robotic Systems (Westminster, MD).

Remote sensing of soil moisture has been performed with sensors mounted to satellites, aerial vehicles, and ground vehicles. Satellite methods of soil moisture estimation use thermal infrared (Wetzel et al., 1984), passive and active microwave (Wigneron et al., 1998; Dubois and van Zyl Engman, 1995), and multi-spectral sensors (Zeng et al., 2004). The satellite methods are useful in characterizing the soil moisture content of large fields, but lack the resolution necessary for detecting small but severe UGV mud hazards. Aerial methods of soil moisture estimation use passive and active

microwave sensors (O'Neill et al., 1996; Archer et al., 2004). Unmanned aerial vehicles (UAVs) with microwave sensors have been used to estimate soil moisture through vegetation clutter (such as a corn field). However, they also lack the resolution for detecting small but severe UGV mud hazards.

Ground vehicle methods of soil moisture estimation have also used passive microwave sensors (Archer et al., 2006). But the antennas tend to be bulky and have been mounted directly downwards, requiring a UGV to drive on potentially hazardous terrain to characterize it. Dupont et al. (2008) classified terrain types, included mud, by using proprioceptive sensors that measure UGV vibration and estimate applied wheel torques. Angelova et al. (2007) developed an algorithm to predict the amount of wheel slippage terrain in the distance will cause using stereo vision sensors. However, these methods also require a UGV to drive on potentially hazardous terrain to characterize or learn about it.

Alshikaili (2007) used a non-contact infrared thermocouple to predict soil moisture content based on soil temperature from a tripod. But a fieldable weather station was required to determine some model parameters (air temperature, solar radiation, relative humidity, wind speed), soil emissivity needed to be manually selected on the thermocouple, and the level of soil compaction needed to be specified. Powers (2008) is experimenting with a monostatic active polarimeter designed to classify solid ground and mud for UGVs. But because there are military operations when it may be desirable for UGVs to operate without emitting strong, detectable electromagnetic signals, a passive perception solution to mud detection is also desirable.

Under the RCTA program, JPL has performed daytime data collections on wet and dry soil using a variety of passive imaging sensors: color stereo, multi-spectral including near-infrared (NIR), short-wave infrared (SWIR), mid-wave infrared (MWIR), long-wave infrared (LWIR), and polarization. In this paper, we examine the cues for mud detection each of these sensors can provide, along with their deficiencies. We started this work focusing primarily on detecting mud where it is most likely to be encountered by a UGV: on dirt trials or open dirt fields. The example in Figure 1 illustrates probably the hardest UGV mud perception scenario; detecting mud when the entire ground is wet and the surface is not soil. Difficult scenarios such as these will be addressed in future work. Here, we mostly limit our examination to mud detection during the daytime under ideal conditions: isolated wet soil surrounded by dry soil during nominal weather, i.e., no precipitation, calm wind, and near average temperatures.

2. MUD CUES FROM COLOR

It is commonly observed that wet soil is considerably darker than dry soil in visible imagery. This is because changing the medium surrounding soil particles from air to water decreases the particle's relative refractive index, increasing the average degree of forwardness of scattering. As a result, incident photons have a higher probability of being absorbed (Twomey et al., 1986). Perrson (2005) found that soil gradually becomes darker as it is wet to a soil moisture level of $0.25\text{m}^3\text{m}^{-3}$ (volume water per unit volume of soil). Beyond that level, some soils start to become lighter again as water starts becoming visible on the surface, causing reflections. As seen in Figure 1, small patches of sitting water tend to be visible when the ground is saturated. These small patches of water are a cue for muddy terrain and can be detected from color analysis if the water is reflecting the sky (Rankin and Matthies, 2006).

The example scenes in Figure 2 illustrate that ground regions significantly darker than surrounding terrain is also a cue for mud. But shadows are also ground regions significantly darker than surrounding terrain. To disambiguate mud from shadows, one can analyze the color content of the dark region. Shadows inherently do not receive direct light from the primary light source. As a result, blue light tends to scatter more relative to red and green light, giving shadows a higher blue saturation than neighboring regions (Wells, 2007). This is illustrated in Figure 3. In the left hue image, the soil in shadow is bluer than non-shadowed soil. In the right image, the non-shadowed mud has the same hue as the surrounding dry soil.

In summary, isolated mud can be detected from color imagery by segmenting regions significantly darker than surrounding terrain (but with the same hue as the surrounding terrain). Extremely muddy terrain can be detected by segmenting small water patches that reflect the sky. Color can also be useful in disambiguating non-shadowed mud from shadows. However, color is probably not very useful in determining if the terrain in a shadow is mud, or in distinguishing the muddiest portion of terrain when the entire ground is wet (except where there are small patches of water reflecting the sky).



Figure 2. Mud tends to be darker than surrounding dry soil in color imagery.

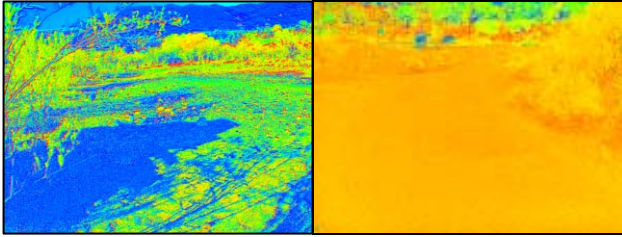


Figure 3. Hue images for the color images in Figure 2. Soil in shadow tends to be bluer than non-shadowed wet or dry soil. But non-shadowed wet soil tends to have the same hue as dry soil.

3. MUD CUES FROM MULTI-SPECTRAL

In the remote sensing community, it is well known that Landsat multi-spectral data on bare soil falls on a line (referred to as the *soil line*) when plotted in NIR vs. red reflectance space. Bare soil pixel placement on the *soil line* depends on soil moisture content. Wet bare soil maps to one end of the line and dry bare soil maps to the opposite end. To determine if this phenomenology is valid from a ground-based sensor, we performed data collections on wet and dry soil with a Duncan Tech MS2100 multi-spectral camera, having spectral sensitivity from 400-1000nm. This camera is based on a color separating prism and three imaging channels that allow simultaneous image acquisition of four spectral bands (red, green, blue, and NIR) through a common aperture.

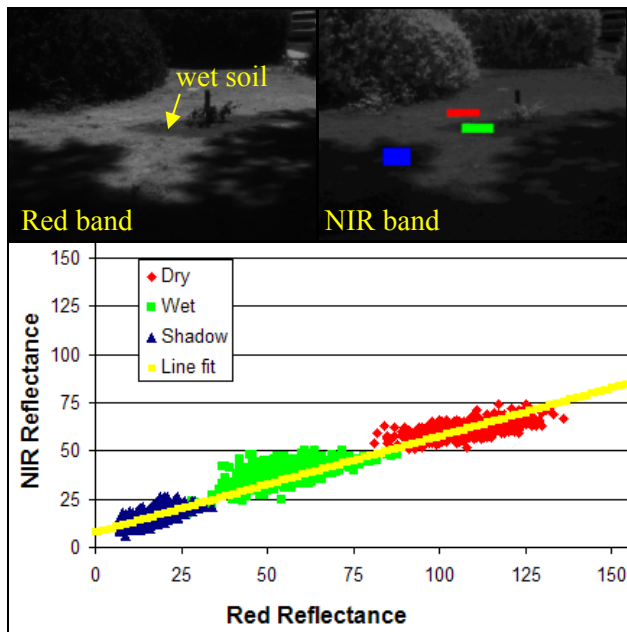


Figure 4. In NIR vs. Red reflectance space, dry, wet, and shadowed soil lies on a line referred to as the *soil line* in remote sensing literature.

Two data collections were performed with the multi-spectral camera mounted to a tripod: one in an area that contained bare soil (both in and out of shadow) and

vegetation, and the second looking down a long dirt road lined with vegetation. Water was poured over a small portion of both scenes and allowed to soak in to the ground. Figure 4 contains images of the red and NIR bands for the first scene. It also contains a NIR vs. red reflectance plot of the pixels in the boxes overlaid on the NIR image. The red box contains dry soil, the green box contains wet soil, and the blue box contains dry soil in shadow. The yellow line is a least squares line fit of the data. From this example, it appears that the *soil line* phenomenology is also valid from a ground-based sensor. Since dry soil in shadow plots to the left of wet soil on the *soil line*, it is more difficult to disambiguate shadows from wet soil than shadows from dry soil.

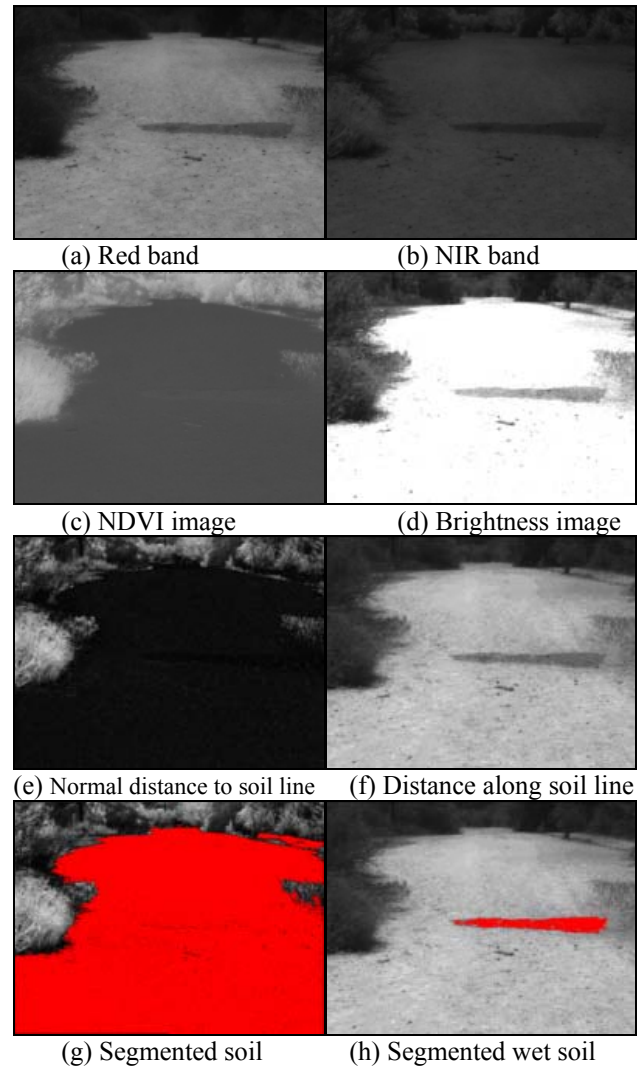


Figure 5. NIR and red bands of a multi-spectral camera may be useful in separating vegetation from soil, and dry soil from wet soil.

Figure 5 illustrates using multi-spectral bands to segment wet soil. Red and NIR bands (Figures 5a and 5b) can be used to generate a Normalized Difference Vegetation Index (NDVI) image (Figure 5c). If the slope

and y-intercept of the *soil line* is known, a *normal distance to the soil line image* (Figure 5e) and a *distance along the soil line image* (Figure 5f) can be generated. The NDVI and *normal distance to the soil line* images can be used to segment soil from vegetation (Figure 5g). A brightness image (Figure 5d), which is derived from the visible bands, and the *distance along the soil line* image can be used to segment wet soil from dry soil (Figure 5h).

Water, snow, and ice all have larger red reflectance values than NIR, bare soil has a slightly larger NIR reflectance than red, and vegetation has a much larger NIR reflectance than red. Some typical NDVI values (from overhead sensors) are 0.7 for dense vegetation, 0-0.1 for bare soil, -0.046 for snow and ice, and -0.257 for water. (Holben, 1986). NDVI is more useful than *distance to the soil line* in segmenting bare soil from vegetation, but *distance along the soil line* is more useful than NDVI in segmenting wet soil from dry soil. However, neither technique is likely to be effective in segmenting snow and ice from mud. *Distance along the soil line* may be useful in segmenting wet soil from soil in shadow, but it is probably not very useful in determining if the soil in shadow is wet or dry.

4. MUD CUES FROM SWIR

Water strongly absorbs light in the NIR and SWIR wavelengths, suggesting that wet soil may also. Lobell and Asner (2002) acquired measurements of reflected shortwave radiation (400-2500nm) of four different soils at varying moisture levels in a laboratory setting using a spectrometer and a calibrated light source. They report that while reflectance for visible wavelength saturates at a soil moisture content of 20%, reflectance for SWIR saturates at a much higher soil moisture content (50%). They concluded that the SWIR region is more suitable for measuring soil moisture content than NIR. The plot in Figure 6 (from Mouazen et al., 2006) illustrates that increasing the soil moisture content causes the largest change in reflectance in a narrow SWIR band near a wavelength of 1450nm. This suggests that passive SWIR should be useful in detecting mud.

We performed data collections on wet and dry soil with a Sensors Unlimited SU320M-1.7RT SWIR camera, to test its feasibility for detecting mud. This camera contains a 320x240 InGasAS detector, spectrally sensitive from 900-1700nm. After acquiring imagery of dry soil, a few buckets of water were poured on the soil. Sample visible and SWIR images from the data collection are shown in Figure 7. As expected, the wet soil is darker than the dry soil in visible and SWIR imagery. We have not yet performed this experiment with varying soil moisture levels. We would expect the wet soil to become progressively darker as the soil moisture content increases.

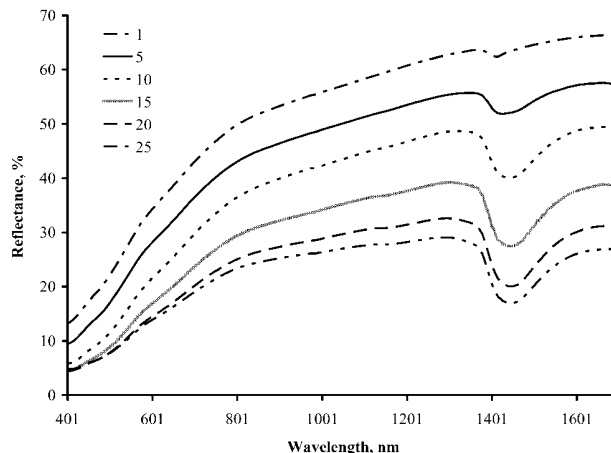


Figure 6. Average spectra recorded for 46 soil samples from a single field (from Mouazen et al., 2006). The curves correspond to soil moisture content, having units of kg kg^{-1} (water mass per unit dry soil mass).

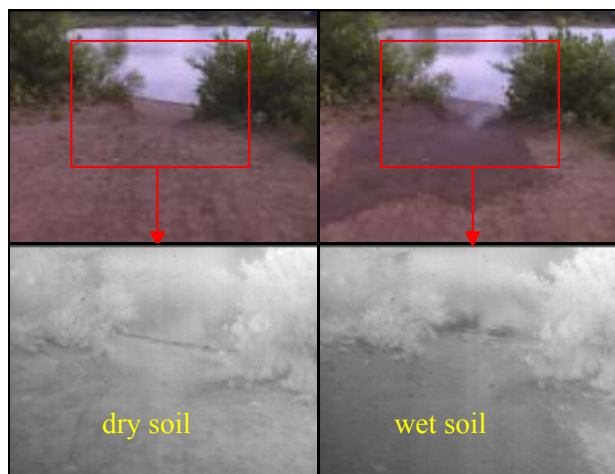


Figure 7. Visible and SWIR imagery of dry and wet soil, acquired from a UGV. The SWIR sensor has a narrower field of view than the visible sensor.

However, not all the dark regions in SWIR imagery are candidate mud. Snow, ice, and water all cause dark regions in SWIR imagery (Matthies et al., 2003). Snow and ice can be distinguished from mud since they are bright in color imagery and mud is not. Water can be distinguished from mud by using color to detect sky reflections and stereo range data to detect terrain reflections (Rankin and Matthies, 2006). Under conditions where the entire ground is wet, if the soil moisture content varies over the terrain, SWIR may be able to indicate the muddiest terrain.

5. MUD CUES FROM THERMAL INFRARED

Factors that influence soil temperature include the angle to the sun, the soil moisture content, if the soil is in shadow, and the time of day. Soil color also influences temperature since darker colors tend to absorb and release energy more rapidly than lighter colors. Wet soil tends to

be cooler than dry soil for a couple of reasons. First, evaporation helps to cool moist soil by dissipating heat. Second, the high heat capacity of water reduces the temperature change from the heat that is absorbed by the soil. (Troeh et al., 2005)

To test the feasibility of using a thermal infrared imaging sensor for mud detection, we performed an all day data collection (6:20am–7:30pm) on a mud body with a Thermoteknix Systems Miricle 110KB long-wave infrared (LWIR) camera, recording images every 20 minutes. This camera has a 384x288 Alpha Silicon micro-bolometer detector with a spectral sensitivity from 7-14 μ m. On the day of this data collection, there was a thick marine layer until 9:20am, it was partially overcast until about 10:00am, and then it was sunny for the remainder of the day.

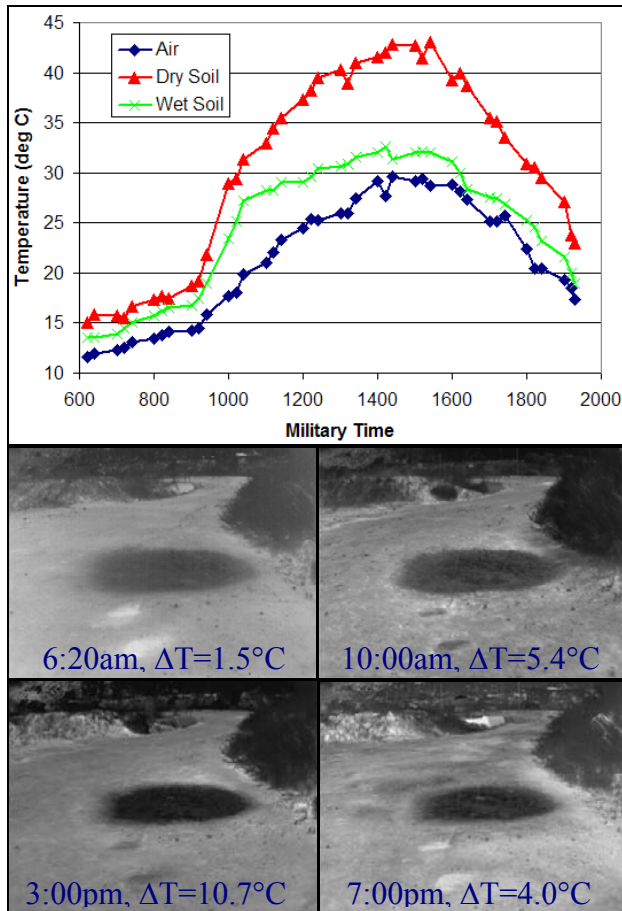


Figure 8. Under nominal weather conditions, mud has a strong signature in LWIR imagery throughout the entire day. ΔT is the difference in temperature between the mud and the surrounding dry soil. This is the same mud body in the right image of Figure 2.

Figure 8 shows a plot of the temperature of the dry soil, mud, and air over the entire day, and sample LWIR images from 6:20am, 10:00am, 3:00pm, and 7:00pm. In the temperature plot, the mud was cooler than the soil

during the entire day, even when there was heavy overcast. The temperature difference between the dry soil and mud started out low in the morning, rose to a peak in the mid afternoon, and started to decline through the evening. The sample imagery confirms that under nominal weather conditions, wet soil is cooler than dry soil throughout the day in thermal infrared imagery. Even at the lowest temperature difference (1.5 $^{\circ}$ C), there was still significant thermal contrast between the dry soil and the mud in the LWIR imagery.

However, not all the dark regions in thermal infrared imagery are candidate mud. Shadows, snow, ice, vegetation, and water can all cause dark regions in thermal infrared imagery. Snow and ice can be distinguished from mud since they are bright in color imagery and mud is not. Tall vegetation can be distinguished from mud by using stereo range data to separate ground clutter from the ground surface. Water can be distinguished from mud by using color to detect sky reflections and stereo range data to detect terrain reflections (Rankin and Matthies, 2006). Figure 9 illustrates that under nominal weather conditions, mud in shadow is cooler than mud out of shadow during the daytime. As discussed in section 2, shadows can be distinguished from non-shadowed mud by analyzing the hue component of color.

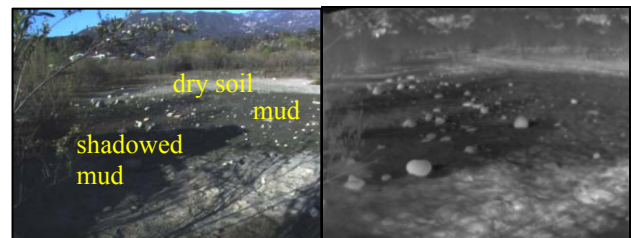


Figure 9. Under nominal weather conditions, mud is cooler than dry soil, and shadowed mud is cooler than non-shadowed mud during the daytime.

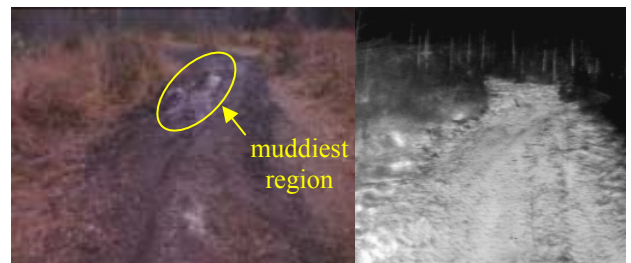


Figure 10. When the entire ground is wet after raining, it would be difficult to use thermal infrared imagery to detect the muddiest portions of the terrain. This color and MWIR image is from Ft. Polk, LA.

Thermal infrared imagery can provide a strong cue for mud during nominal weather conditions when non-mud dark regions are disambiguated with other sensors. But under off-nominal conditions, such as after

precipitation when the entire ground is damp, the usefulness of thermal infrared imagery for mud detection decreases. As illustrated with the mid-wave infrared (MWIR) image in Figure 10, it is difficult to detect the muddiest portions of the road from the rest of the wet road in thermal infrared imagery. If the soil moisture content varies over the terrain, SWIR may help in such situations.

6. MUD CUES FROM POLARIZATION

There are four fundamental properties of light: intensity, wavelength, coherence, and polarization. In the past, vision-based terrain classification methods have focused primarily on intensity and wavelength (color) properties. But with the recent emergence of polarization cameras, the components of polarization from light reflected off surfaces can also be exploited to classify terrain types. For example, Xie et al. (2007) and Pandian (2008) have recently experimented with using a polarization camera to detect water.

Almost all naturally occurring outdoor light (scattered and reflected) is at least partially linearly polarized (Wolff, 2005). At a pixel level, partial linear polarization is measured by the transmitted radiance through a polarization filter. To determine the whole partial linear polarization state [orientation, intensity, and degree of linear polarization (DOLP)], three images of a scene needs to be acquired, each with the polarization filter at a different orientation. The DOLP at each pixel is a value between 0 (completely unpolarized light) and 1 (completely linear polarized light).

To calculate a simplified polarization measure called *polarization contrast*, only two images of a scene are required, as long as the polarization filter orientations differ by 90°. If one of the filter orientations is aligned with the orientation of the linearly polarized component in the input light, then *polarization contrast* equals DOLP. Otherwise, *polarization contrast* provides a lower bound for DOLP (Pandian, 2008). Since water and mud appear to be horizontally polarized, if filter orientation angles of 0° (*crossed*) and 90° (*parallel*) are chosen, *polarization contrast* can be used to estimate DOLP on water and mud. The *polarization contrast* at each pixel can be calculated by dividing the absolute value of the difference between the *parallel* and *crossed* intensity values by the sum of the *parallel* and *crossed* intensity values.

Regions of a natural terrain scene that have a significantly higher DOLP than surrounding terrain can be a potential cue for water. However, the DOLP of reflections from water bodies is a function of the incidence angle, hence lookahead distance. Moreover, it will also be affected by the polarization of the light incident on the water, which is dependent on sky

conditions, sun position, and viewing geometry, as well as on the polarization of light upwelling from within the water body. Therefore, there are conditions where the DOLP on water will not be significantly higher than surrounding terrain. As an example, Xie et al. (2007) found that water reflecting nearby vegetation had a DOLP almost the same as the surrounding terrain.

To determine if there is a polarization signature on wet soil useful to detecting mud, several daytime data collections were performed with two Bossa Nova Technologies sensors: a SAMBA polarization camera and a SALSA linear stokes polarization camera. The SAMBA camera provides a *polarization contrast* image and the SALSA camera provides DOLP, intensity, and orientation images. In the first data collection, SAMBA polarization imagery of a single mud body was acquired every 20 minutes for over seven hours from a stationary position with the sensor facing northeast. The data collection started at 6:20am and ended at 1:40pm. A full day data collection was planned, but a portable generator that provided power to the hardware failed near the half way point.

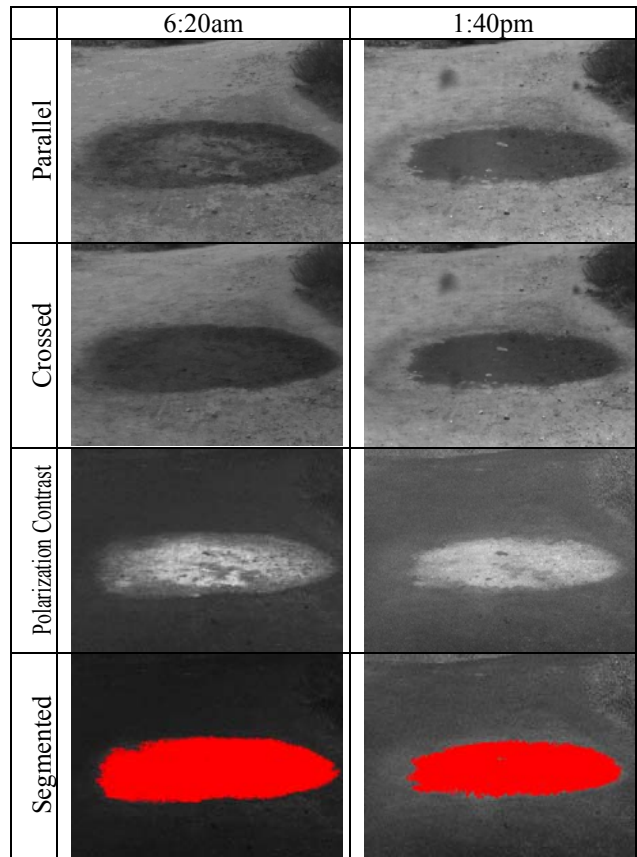


Figure 11. Segmenting mud using SAMBA polarization imagery at different times of the day.

A circular region of soil having a radius of approximately 2 meters was periodically watered for three days prior to the data collection to ensure a mud

consistency. There was a thick marine layer at the beginning of the data collection, but by 9:20am, the sun started to peek through it, and by 10:00am, it had completely evaporated. The *polarization contrast* on the mud was significantly higher than the surrounding dry soil in all the samples. Figure 11 shows the *parallel* and *crossed* polarization images, the resultant *polarization contrast* images, and segmented mud images for the first and last images from the data collection. The same parameters were used to segment the mud at both times.

In a second data collection, a color camera and SALSA polarization camera were mounted to the hood of a vehicle and a mud body was imaged from three different directions (facing West, South, and East). This data collection took place at approximately 10:00am on an overcast day. Each image was taken minutes apart from the previous image. As illustrated in Figure 12, in all three cases, the DOLP on the mud was consistently higher than the surrounding dry soil.


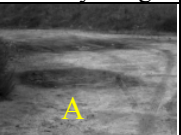
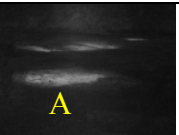


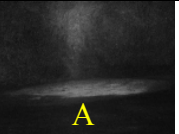


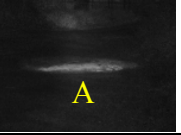
	RGB image	Polarization intensity image	DOLP
West			
South			
East			

Figure 12. A mud body (A) imaged on an overcast day from three directions with a color and SALSA polarization camera. The images for each heading were acquired a few minutes apart. The DOLP on mud is consistently high, independent of sensor orientation.

The DOLP on water can change based on the sky conditions, the sun position, and the sensor orientation. But the DOLP on wet soil appears to be consistently high, regardless of those conditions. This is illustrated in Figure 13, which contains a *parallel* polarization image (left) and the corresponding *polarization contrast* image (right). The scene contains sitting water, wet soil, dry soil, and vegetation. While the DOLP of the sitting water is much lower than the dry soil, the DOLP of the wet soil is much higher than the dry soil. Even mud driven over by vehicles has a higher DOLP than surrounding dry soil (Figure 14).

There is one case, however, where we have observed a weak polarization signature on wet soil. As illustrated in Figure 15, the DOLP on wet soil in shadow is very similar to the DOLP of dry soil in shadow. In addition, water and mud cannot be distinguished solely using DOLP. Water can be distinguished from mud by using color to detect sky reflections and stereo range data to detect terrain reflections (Rankin and Matthies, 2006).

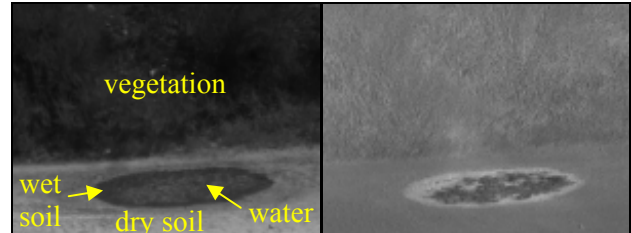


Figure 13. A SAMBA parallel and polarization contrast image. The DOLP on water can change based on if the sun is out, the sun position, and the sensor orientation. But the DOLP on wet soil appears to be consistently high, regardless of those conditions.

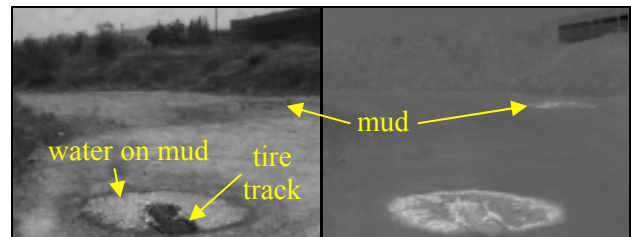


Figure 14. A SAMBA parallel and polarization contrast image. Mud that has been driven over has a high DOLP.

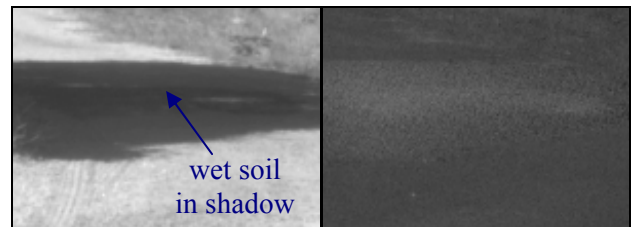


Figure 15. A SALSA intensity and DOLP image. The DOLP of wet soil in shadow is similar to the DOLP of the dry soil in shadow.

7. MUD LOCALIZATION IN A TERRAIN MAP

Mud detected onboard a UGV should be placed within the world map the UGV uses to plan safe paths. In this section, we illustrate the process with a multi-sensor based mud detection solution. A SALSA polarization camera was used to detect mud and a stereo pair of Hitachi HV-F31 color cameras was used to localize detected mud and reject false alarms. The first row of Figure 16 shows the sensors mounted to the hood of a High Mobility Multi-Wheeled Vehicle (HMMWV). The stereo baseline was 50cm. All three sensors were

calibrated within the vehicle frame. The HMMWV was manually driven towards the mud body shown in the upper left image. The images in rows 2-4 are from one frame of data during the drive, illustrating mud detection from a range of 27 meters.

A mud detection algorithm was implemented which thresholds DOLP and back-projects polarization pixels that have a high DOLP into the left color image (which is registered with the stereo range image). The last row of Figure 16 shows the mud detection results in the stereo point cloud. As illustrated by the bird's-eye view of the world map, mud detection and elevation data are accumulated over time in a north oriented grid map containing 40cm resolution cells. Dark blue indicates the location of detected mud, cyan indicates the vehicle path, white indicates cells that have no data, and the gray level represents elevation (where black is high elevation). As we only expect mud to occur on the ground, stereo vision can be used to isolate ground pixels from the other pixels corresponding to ground clutter. For this particular scene, vegetation with a high DOLP was not placed within the world map since those pixels are above the ground. We have not implanted color analysis yet, which will improve the robustness of this detector.

CONCLUSIONS

Robust mud detection is a critical perception requirement for UGV autonomous navigation. There are several characteristics of mud that may be detectable with appropriate sensors. For example, mud only occurs on the ground surface, mud is usually cooler than surrounding soil during the daytime, mud is generally darker than surrounding soil in visible imagery, and mud is highly polarized. None of these cues, however, is definitive on its own. Dry soil also occurs on the ground surface, shadows are also cooler than surrounding soil, shadows are also darker than surrounding soil in visible imagery, and cars, water, and some vegetation are also highly polarized. Thus, a multi-sensor approach to mud detection is desired.

A passive mud detection solution is desirable to meet the Future Combat System Autonomous Navigation System (FCS-ANS) requirements. Under the ARL RCTA program, JPL has performed daytime data collections on wet and dry soil using a variety of passive sensors including color stereo, multi-spectral (visible plus NIR), SWIR, MWIR, LWIR, and polarization. In this paper, we have described the cues for mud detection that several of these passive sensors can provide under ideal daytime conditions (isolated wet soil surrounded by dry soil during nominal weather), and a method for localizing mud hazards in a world map using stereo vision.

During FY09, we are planning on fusing cues from color into the current mud detector, and implementing a

second mud detector that fuses cues from color, stereo, and thermal infrared. More work is needed to characterize the usability of the sensors evaluated in this paper to detect mud under non-ideal conditions.

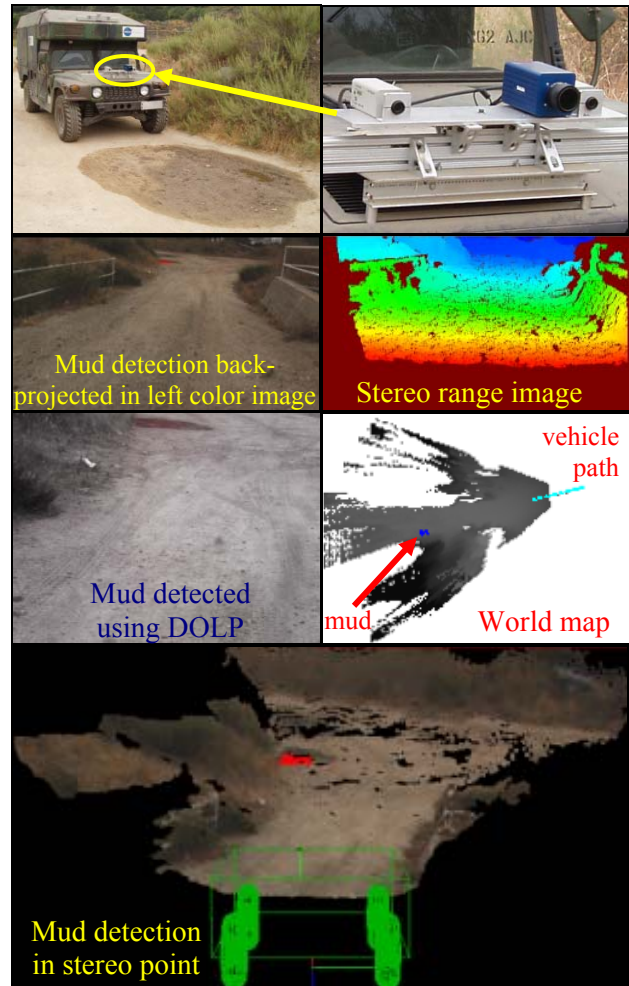


Figure 16. Localizing detected mud in a world model using a stereo pair of color cameras.

ACKNOWLEDGEMENTS

The research described in this paper was carried out by JPL, California Institute of Technology, and was sponsored by the ARL RCTA program through an agreement with the National Aeronautics and Space Administration. Reference herein to any specific commercial product, process, or service by trademark, manufacturer, or otherwise, does not constitute or imply its endorsement by the United States Government or JPL, California Institute of Technology.

REFERENCES

Alshikaili, T.Y., 2007: "Non-Contact Measurement of Soil Moisture Content using Thermal Infrared Sensor

- and Weather Variables”, *Masters Thesis*, University of Saskatchewan, Saskatoon, Saskatchewan.
- Angelova, A., Matthies, L., Helmick, D., and Perona, P., 2007: “Learning and Prediction of Slip from Visual Information”, *Journal of Field Robotics*, **24(3)**, 205-231.
- Archer, F., Shutko, A.M., Coleman, T.L., Haldin, A., Novichikhin, E., Sidorov, I., 2004: “Introduction, Overview, and Status of the Microwave Autonomous Copter System (MACS)”, *Proceedings of the IEEE International Symposium on Geoscience and Remote Sensing*, **5**, 3574-3576.
- Archer, F., Shutko, A., Coleman, T.L., Haldin, A., Sidorov, I., and Novichikhin, E., 2006: “Microwave Remote Sensing of Soil Moisture from a Rover and Robotic Aerial Platform: The Alabama Experiments”, *Proceedings of the 18th World Congress on Soil Science*, Philadelphia, PA.
- Dubois, P.C., and van Zyl Engman, J., 1995: “Measuring Soil Moisture with Imaging Radars”, *IEEE Trans. Geosci. Remote Sensing*, **33(4)**, 915-926.
- DuPont, E.M., Collins, E.G., Coyle, E.J., and Roberts, R.G., 2008: Terrain Classification using Vibration Sensors: Theory and Methods. In: *New Research on Mobile Robotics*, Davies and Hall (eds.), Nova Science Publisher Inc., Hauppauge, NY.
- Hamrita, T.K., Tollner E.W., and Schafer, R.L., 2000: “Toward Fulfilling the Robotic Farming Vision: Advances in Sensors and Controllers for Agricultural Applications”, *IEEE Transactions on Industry Applications*, **36(4)** 1026-1032.
- Holben, B.N., 1986: “Characteristics of Maximum-Value Composite Images from Temporal AVHRR Data”, *IJRS*, **7(11)**, 1417-1434
- Lobell, D.B., and Asner, G.P., 2002: “Moisture Effects on Soil Reflectance”, *Soil Sci. Soc. Am. J.*, **66**, 722-727.
- Matthies, L., Bellutta, P., and McHenry, M., 2003: “Detecting Water Hazards for Autonomous Off-Road Navigation”, *Proceedings of SPIE Conference 5083: Unmanned Ground Vehicle Technology V*, Orlando, 231-242.
- Mills, M.E., 2007: “Challenges to the Acceptance and Proliferation of Tactical UGVs”, *RUSI Defence Systems*, October, 28-30.
- Mouazen, A.M., Karoui, R., De Baerdemaeker, J., Ramon, H., 2006: “Characterization of Soil Water Content using Measured Visible and Near Infrared Spectra”, *Soil Sci. Soc. Am. J.*, **70**, 1295-1302.
- O’Neill, P., Chauhan, N., Jackson, T., 1996: “Use of Active and Passive Microwave Remote Sensing for Soil Moisture Estimation Through Corn”, *Int. J. Rem. Sens.*, **17(10)**, 1851-1865.
- Pandian, A., 2008: “Robot Navigation using Stereo Vision and Polarization Imaging”, *Masters Thesis*, Institut Universitaire de Technologie IUT Le Creusot, Universit_e de Bourgogne.
- Persson, M., 2005: “Estimating Surface Soil Moisture from Soil Color using Image Analysis”, *Vadose Zone J.*, **4**, 1119-1122.
- Powers, M., 2008: “Next Generation Sensors for Autonomous Mobility”, *Robotics Collaborative Technology Alliances Interim Program Review*, Aberdeen, MD, August 5-7, 2008.
- Rankin, A., and Matthies, L., 2006: “Daytime Water Detection and Localization for Unmanned Vehicle Autonomous Navigation”, *Proceedings of the 25th Army Science Conference*, Orlando, FL.
- Sudduth, K.A., Hummel, J.W., and Birrell, S.J., 1997: Sensors for Site-Specific Management. In: *The State of Site-Specific Management for Agriculture*, Chapter 10, pp. 183-210, Pierce and Sadler (eds.), ASA-CSSA-SSSA, Madison, WI.
- Troeh, F.R., and Thompson, L.M., 2005: *Soils and Soil Fertility*, Blackwell Publishing, Boston.
- Twomey, S.A., Bohren, C.F., and Mergenthaler, J.L., 1986: “Reflectances and Albedo Differences between Wet and Dry Surfaces”, *Appl. Optics* **25**, 431-437.
- Wells, B., 2007: “Detection and Manipulation of Shadows in an Image or Series of Images”, U.S. Patent #7305127, December 4, 2007.
- Wetzel, P.J., Atlas, D., Woodward, R., 1984: “Determining Soil Moisture from Geosynchronous Satellite Infrared Data: A Feasibility Study”, *Journal of Climate and Applied Meteorology*, **23**, 375-391.
- Whalley, W.R. and Stafford, J.V., 1992: “Real-Time Sensing of Soil Water Content from Mobile Machinery: Options for Sensor Design”, *Comput. Electron. Agri.*, **7(4)**, 269-284.
- Wigneron, J.P., Schmugge, T., Chanzy, A., Kerr, C.Y., 1998: “Use of Passive Remote Sensing to Monitor Soil Moisture”, *Agronomia*, **18**, 27-43.
- Wolff, L.B., 2005: “Applications of Polarization Camera Technology”, *IEEE Expert: Intelligent Systems and their Application*, **10(5)**, 30-38.
- Xie, B., Xiang, Z., Pan, H., and Liu, J., 2007: “Polarization-based Water Hazard Detection for Autonomous Off-Road Navigation”, *Proceedings of the IEEE/RSJ International Conference on Intelligent Robots and Systems*, San Diego, CA, 3186-3190.
- Zeng, Y., Feng, Z., and Xiang, N., 2004: "Assessment of Soil Moisture using Landsat ETM+ Temperature/Vegetation Index in Semiarid Environment," *Proceedings of the IEEE International Geoscience and Remote Sensing Symposium*, **(6)**, 4306-4309.